Journal of Nuclear Materials 455 (2014) 5–9

Contents lists available at ScienceDirect

Journal of Nuclear Materials

journal homepage: www.elsevier.com/locate/jnucmat

Synergetic effects of Mn and Si in the interaction with point defects in bcc Fe

A. Bakaev [a,b,c,*], D. Terentyev [a], X. He [d], D. Van Neck [b]

[a] SCK•CEN, Nuclear Materials Science Institute, Boeretang 200, Mol B2400, Belgium
[b] Center for Molecular Modeling, Department of Physics and Astronomy, Ghent University, Technologiepark 903, 9052 Zwijnaarde, Belgium
[c] Department of Experimental Nuclear Physics, Institute of Physics, Nanotechnologies and Telecommunications, St. Petersburg State Polytechnical University, 29 Polytekhnicheskaya Str., 195251 St. Petersburg, Russia
[d] China Institute of Atomic Energy, PO Box 275-51, 102413 Beijing, China

ARTICLE INFO

Article history:
Available online 5 March 2014

ABSTRACT

The interaction of Mn, Si and Cr with a vacancy and self-interstitial defects in BCC Fe has been analyzed using *ab initio* calculations. While the interaction of the considered solute clusters with a single vacancy is linearly additive, there is a considerable synergetic effect in the case of self-interstitial atoms, found to bind strongly with Mn–Si pairs. The latter therefore act as deep trapping configurations for self-interstitials. At the same time, the presence of the point defects nearby weakly attractive Mn–Si pairs significantly enhances the solute–solute binding. The revealed effects are rationalized on the basis of charge density and local magnetic moment distributions.

1. Introduction

Fe–Cr-based ferritic steels are considered as candidate materials for Generation IV and fusion installations [1]. Radiation induced degradation of high-Cr ferritic steels is an important factor limiting the temperature window for applications and the operational time span. This is why the significant efforts are dedicated to understand the origin and evolution of radiation induced defects causing the hardening [2,3].

A series of recent works, where the post irradiation experimental analysis of several Fe–Cr model alloys has been performed [4–6], reveal the numerous formation of Cr–Si clusters (also containing Ni and P but in less quantities than Cr and Si) with a number density of 10^{23} m^{-3} and mean radius of ~(1.5–2.5) nm, which cannot be classified as α' precipitates because of too low Cr content in them. Radiation induced segregation is most likely to be responsible for their formation as the composition of Si in the considered alloys is less than 0.5 at.% i.e. far below its solubility limit in Fe at 300 °C of 10 at.%.

Although the content of Mn (well below the solubility limit in α-Fe [7] at 300 °C) and Si in high-Cr steels is rather low (up to 0.5 wt.%), atom probe studies performed in irradiated commercial ferritic–martensitic steels also revealed the formation of Mn–Si clusters (also containing Ni) [8] with a similar density and size as in [5]. The scenario by which these clusters are formed and how they contribute to hardening in high-Cr steels is so far unclear. Assuming that radiation induced/enhanced segregation is responsible for the occurrence of the above discussed solute-rich clusters, investigation of the interaction of these solutes with point defects (PDs) is the first step.

The interaction of PDs with a single solute atom (Cr, Mn, Si) was extensively studied using *ab initio* techniques in the past [9–14]. The results of these calculations can be summarized as follows:

(i) Mn exhibits attractive interaction with both vacancy and self-interstitial atom (SIA), and it forms a highly stable mixed ⟨1 1 0⟩ split dumbbell. The migration of the mixed Fe–Mn dumbbell via displacement of Mn occurs with the same migration energy [12] as that for an Fe–Fe dumbbell (i.e. 0.34 eV [15]). Hence, Mn can be transferred via SIA defects. The vacancy-Mn exchange (1.03 eV [16]) requires a higher energy barrier than the vacancy migration energy in pure Fe (i.e. 0.65 eV [17]).
(ii) Si is strongly bound to a vacancy and this binding cannot be explained on the basis of lattice-strain compensation so originates from the magnetic relaxation [13]. The migration barrier for Si-vacancy exchange (0.44 eV [16]) is lower than the vacancy migration energy in pure Fe [16]. Si is also attracted to an FeFe and FeCr ⟨1 1 0⟩ split dumbbell (henceforth dumbbell) being placed in the nearest compression site

* Corresponding author at: SCK•CEN, Nuclear Materials Science Institute, Boeretang 200, Mol B2400, Belgium. Tel.: +32 14 33 30 89.
E-mail address: abakaev@sckcen.be (A. Bakaev).

http://dx.doi.org/10.1016/j.jnucmat.2014.02.033
0022-3115/

[14]. The migration barrier for Si in the mixed dumbbell is found to be 0.52 eV [12], which is essentially higher than the SIA migration energy in bcc Fe. Si atoms are therefore expected to be transported by vacancy diffusion mechanism only.

The interaction of multiple solute-PD clusters involving Mn, Si and Cr (the latter being the major alloying element in high-Cr steels) has not been studied so far. Our recent work [14] has clearly shown that Mn and Si are the two outstanding elements entering the composition of high-Cr steels in terms of the interaction with important lattice defects such as: the self-interstitial atom, a high angle grain boundary, a ½⟨1 1 1⟩ screw dislocation core and an interstitial carbon atom. Here, we perform a dedicated *ab initio* study looking for a possible synergy between Mn, Si and Cr simultaneously interacting with PDs attempting to provide some evidence of the enhanced Mn–Si or Cr–Si binding, following the evidence from the above mentioned experiments. Given that in Fe–Cr–Mn–Si alloys the formation of mixed Fe–Cr and Fe–Mn dumbbells is energetically favourable [9,10], the interaction of the mixed SIAs with an isolated Mn or Si atom and with Mn–Si pairs is also addressed to highlight the possible trapping effect originating from the multiple solute-PD interaction.

2. Computational details

The DFT calculations were performed with the Vienna Ab Initio Simulation Package VASP [18,19] using the projector-augmented wave (PAW) potentials [20,21]. The electron exchange–correlation functional was described within the generalized gradient approximation using PW91 functionals [22], with a Vosko–Wilk–Nusair interpolation [23]. For Fe, Cr, Mn and Si pseudo potentials with 8, 6, 7 and 4 valence electrons were used, respectively. Ionic relaxation was performed using the conjugate gradient algorithm with a force convergence criterion of 0.03 eV/Å. By default all the calculations were done keeping the cell shape and volume (equal to the equilibrium volume of bulk iron) constant to provide the results fully compatible with the set of previous DFT works [9–14]. The lowest energy configurations for several PD-solutes structures were re-relaxed performing the cell shape and volume optimization to ensure the convergence of the interaction energies obtained using constant volume calculations. The energy cutoff for calculations was 300 eV which was proven to be enough to provide converged results [24]. A $3 \times 3 \times 3$ k-point mesh was sampled by the Monkhorst and Pack scheme for systems with 128 atoms. The lattice parameter of pure ferromagnetic Fe is taken to be 2.831 Å following the previous studies [9,14,24].

Given that we perform spin-polarized calculations in the ferromagnetic system and introduce anti-ferromagnetic impurity (i.e. Mn), one needs to be careful when selecting the initial value of the magnetic moment to ensure that the minimum energy configuration is obtained after the relaxation. In the calculations involving Mn, when its magnetic spin was not anti-ferromagnetic to Fe after the relaxation, we performed additional calculations varying the absolute value of the initial moment as some of the results turned out to be particularly sensitive to the choice of the initial magnetic moment. Below, we report only the results corresponding to the lowest energy configurations found.

To assess the interaction energy we apply the standard definition conventionally used in many similar DFT works [10]. The interaction energy of n defects $\{A_i\}$ is defined as [10]:

$$E_i(\{A_i\}) = [E(\{A_i\}) + (n-1)E_0] - \left[\sum_{i=1}^{n} E(A_i)\right], \quad (1)$$

where $E(A_i)$ is the energy of the configuration containing A_i only, $E(\{A_i\})$ is the energy of the configuration with all the n defects, and E_0 refers to a configuration containing no defects or impurities, i.e. bulk bcc iron. Following this notation, a negative value implies an attractive interaction and vice versa.

To assess a possible synergetic interaction of the solutes with PDs we have applied the following strategy.

Firstly, the energetically stable (in terms of the binding energy) pairs of solute atoms (i.e. Mn–Cr, Mn–Si, Cr–Si) with the distances up to 5th nearest neighbor (nn) were identified. It is worth mentioning that alike solutes were found to strongly repel each other in the 1st and 2nd nearest neighbor positions, and the repulsion vanished in the 3rd coordination shell [10,14]. Mn–Mn is the only exception, as two substitutional Mn atoms were found to attract each other in the 1st position with the interaction energy of −0.26 eV [14]. In this work we considered cross pairs only. Then, once the attracting solute pairs were defined, we have constructed several Mn–Cr–Si clusters searching for the most favourable arrangements. After that, the configurations involving the studied PDs interacting with either a single, pair or triplet cluster were constructed and relaxed.

Using the data on the total energy of the relaxed crystals containing either the solute clusters or solute-PD clusters, we computed the interaction energy of the PDs with a single solute, pair and triplet of solutes, henceforth referred to as E_I(PD-S1), E_I(PD-S1&S2) and E_I(PD-S1&S2&S3). The synergetic effect could therefore be revealed by comparing E_I(PD-S1&S2) and E_I(PD-S1) + E_I(PD-S2) + E_I(S1–S2), where the latter is a linear superposition of the interaction energies. A schematic representation of the explored configurations involving SIAs and vacancies is given in Fig. 1 (see figure caption for detailed explanation).

3. Results

Among the considered solutes cross pairs, only Mn–Si atoms were found to bind with each other in the 1st nn, see Fig. 2. Mn–Mn solute interaction energy is shown for comparison and is taken from [14]. The resulting Mn–Si (1st nn) interaction energy is −0.09 eV. It is worth to mention that in all the studied configuration the magnetic moment of Mn was negative (opposite to the one of Fe) with the only exception of Mn–Si 2nd nn configuration where the magnetic moment of Mn in the lowest energy configuration turned out to be positive +1.2μ_B. However, the difference in the total energy between configurations in which the Mn

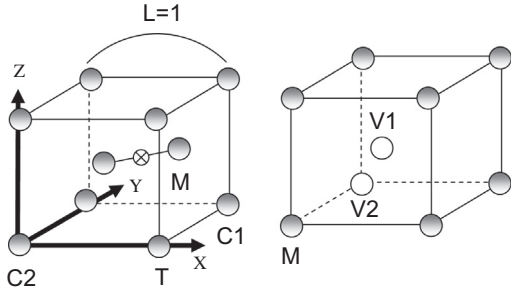

Fig. 1. The studied atomic configurations. The left figure shows non-equivalent sites around a ⟨110⟩ split dumbbell, namely: M is a position of solute in a mixed dumbbell; C1 and C2 are the sites in the compression region of the dumbbell strain field; T is the site located in the tensile region of the dumbbell strain field. The position of the second solute was defined relative to the center of the box (marked with cross) taking a lattice spacing as unity. The right figure shows the considered configurations with vacancies. M points at a position of the first solute atom. V1 and V2 are the two considered positions for the vacancy. The orientations of *X*, *Y* and *Z* axes are [100], [010] and [001], respectively, for both right and left figures.

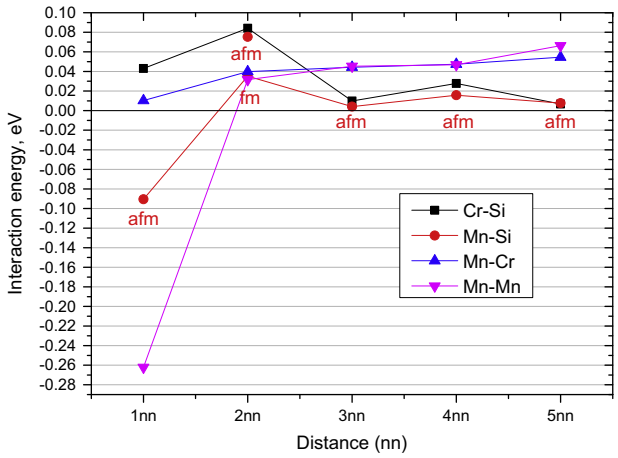

Fig. 2. Interaction energy of the solute pairs. 'fm' points to ferromagnetic (coaligned with Fe atoms) and 'afm' – to antiferromagnetic spin orientation of Mn (in the case of Mn–Si pair), respectively.

magnetic moment was co- and anti-aligned (with $-2.1\mu_B$) is only 0.04 eV.

Note that according to the calculations utilizing the ultrasoft pseudopotential (USPP) method [16], the Mn–Si interaction is practically negligible in the 1st nn (−0.01 eV) and is strongly repulsive in the 2nd nn (0.33 eV) positions. However, the USPP method is believed to be less accurate when the ferromagnetic system is concerned.

Studying the triple solute clusters, we could not find an arrangement having a negative total interaction energy. Out of all studied configurations, the cluster combining Cr, Mn and Si atoms, placed in the 1st nn relative to each other (e.g. in positions Cr = 0.5;0.5;0.5, Mn = 0.0;0.0;0.0 and Si = −0.5;0.5;0.5), corresponds to the lowest energy structure with the interaction energy of +0.06 eV. Hence, the 1st nn Mn–Si and Mn–Mn pairs are the only solute arrangements revealing considerable binding.

The interaction energy for point defects (vacancy, Fe-solute and FeFe dumbbells) associated with either a single or a pair of solutes are reported in Table 1. The difference $\Delta E = E_I(\text{PD-S1\&S2}) - E_I(\text{PD-S1})$ is also reported in the table to indicate the added strength due to the inclusion of the 2nd solute. Since only the Mn–Si cross pair was found to bind in substitutional positions, it is of interest to discuss how the presence of the PDs affects its binding. E_I(PD-S1&S2) varies from −0.09 down to −0.78 eV, implying that the Mn–Si binding is enhanced by the PDs in all the configurations presented in Table 1. Finding E_I(PD-S1&S2) close to zero corresponds to no enhancement of the Mn–Si binding, while a negative value points at the binding increase. A vacancy or FeFe dumbbell inserted nearby the Mn–Si pair increases its interaction energy, respectively, by 0.25–0.34 eV and 0.17–0.39 eV, depending on a specific local arrangement. The strongest effect however is observed in the case of the interaction of Fe–Mn dumbbell with Si solute, which increases the Mn–Si binding energy by 0.78 eV. This strongly bound configuration may occur by either association of the migrating Fe–Mn dumbbell with an isolated substitutional Si, or coalescence of the migrating FeFe dumbbell with the 1st nn Mn–Si pair (resulting in the transformation of FeFe into Fe–Mn dumbbell).

The revealed strong binding of the Mn–Si pair with PDs implies that these solutes can also be considered as traps for mobile PDs. Among the PDs listed in Table 1, only the FeSi dumbbell is immobile, as the dissociation from Si followed by the migration of an FeFe dumbbell is expected [12]. The trapping effect of the Mn–Si pair is the most striking in the case of FeMn dumbbells (see E_I(FeMn + Si) in Table 1), for which the binding energy goes up to −0.78 eV, while FeFe and FeCr dumbbells are bound with an energy up to −0.41 eV. The binding of the Mn–Si pair with a vacancy is even weaker and it reaches −0.34 eV in the lowest energy configuration found.

The addition of the second solute (either Mn or Si) to a PD-S1 configuration increases the total interaction energy i.e. E_I(PD-S1&S2) in all configurations except for FeCr + Mn + Si. However, the added binding energy (ΔE) is of the order of the Mn–Si interaction energy, being ∼0.1 eV, which points to the linearly additive interaction character of the PDs with the solutes. Only two

Table 1
Interaction energy of PD-solute configurations. E_I(PD-S1&S2) is the interaction energy of PD with the S1&S2 complex. E_I(PD-S1) is the interaction energy of PD with S1 solute. The interaction energy of a FeS1–S2 configuration was calculated with respect to dissociation to Fe–Fe + S1–S2 clusters. FeFe, FeCr, FeMn, FeSi and MnCr denote ⟨1 1 0⟩ dumbbell configurations of different chemistry. The second solute atom (S2) was everywhere added in the 1st nn position to the first solute atom (S1). The coordinates of the S2 are given in the 5th column, the coordinate system is provided in Fig. 1. The energy marked with "*" is obtained using the cell volume/shape relaxation where in all the other configurations cell volume/shape were kept constant.

Configuration: defect + S1 + S2	E_I(PD-S1&S2) (eV)	E_I(PD-S1) (eV)	ΔE (eV)	Equivalent positions of the S2, see Fig. 1.
FeCr + Si(C2) + Mn	−0.41	−0.30	−0.11	−1.0;0.0;0.0 0.0;−1.0;0.0
FeCr + Mn(C2) + Si	−0.40	−0.30	−0.10	−1.0;0.0;0.0 0.0;−1.0;0.0
MnCr + Si	−0.29	−0.24	−0.05	−0.5;−0.5;−0.5(C2)
FeCr + Mn(C1) + Si	−0.09	−0.12	0.03	0.0;1.0;0.0 1.0;1.0;−1.0 1.0;0.0;0.0
FeCr + Mn(T) + Si	−0.08	−0.01	−0.07	0.0;−1.0;0.0
Vac + Si(1nn) + Mn	−0.34	−0.31	−0.03	−1.0;0.0;0.0 0.0;0.0;−1.0 0.0;−1.0;0.0
Vac + Mn(1nn) + Si	−0.25	−0.17	−0.08	−1.0;0.0;0.0 0.0;0.0;−1.0 0.0;−1.0;0.0
FeMn + Si	−0.78 (−0.77*)	−0.59 (−0.57*)	−0.19	−0.5;−0.5;−0.5 (C2)
FeSi + Mn	−0.42	0.00	−0.42	−0.5;−0.5;−0.5 (C2)
FeFe + Mn(C) + Si	−0.39	−0.32	−0.07	0.0;1.0;0.0 1.0;0.0;0.0
FeFe + Si(C) + Mn	−0.37	−0.28	−0.09	0.0;1.0;0.0 1.0;0.0;0.0
FeFe + Mn(T) + Si	−0.17	−0.09	−0.08	1.0;0.0;0.0 0.0;−1.0;0.0

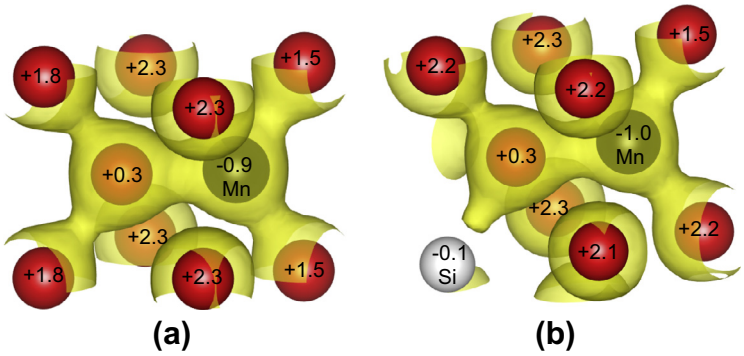

Fig. 3. Distribution of charge density around a ⟨1 1 0⟩ split dumbbell in a eight atom bcc cell. Isosurfaces of 0.55 e/Å^3 are shown. The color of the atom refers to its type: red – Fe, black – Mn, white – Si. (a) and (b) figures correspond to FeMn (⟨1 1 0⟩ dumbbell) and FeMn (⟨1 1 0⟩ dumbbell) + Si(C2) complexes, respectively. (For interpretation of the references to colour in this figure legend, the reader is referred to the web version of this article.)

configurations reveal a remarkable gain in the total energy after the addition of the second solute. These are FeMn and FeSi dumbbells placed in the vicinity of a Si or Mn atom, respectively. In those cases, ΔE is −0.19 eV and −0.42 eV, respectively.

The configuration involving the FeMn dumbbell corresponds to the lowest total energy state, therefore, we focus on its properties to explain the origin of the observed synergetic effect. To do that we have computed the local magnetic moments of all atoms and analyzed the distributions of the charge density in the two configurations, namely: FeMn dumbbell and FeMn dumbbell standing next to Si in the C2 site (see Fig. 1). The change of magnetic moments in FeMn to FeMn + Si (1nn) complexes is shown in Fig. 3 also revealing the charge density distribution. The Fe in the FeMn dumbbell is bonded with two adjacent Fe atoms (see Fig. 3a). The substitution of Fe by Si results in the shift of position of the Fe atom (forming the dumbbell) down by $-0.016 \times a_0$ towards Si atom. That causes a slight on site rotation of the dumbbell axis. At the same time, the introduction of diamagnetic Si instead of ferromagnetic Fe leads to a strong redistribution of the charge density (see Fig. 3b), which apparently causes the recovery of the magnetic moments of the Fe atoms located in the two compression sites (C1 and the site above Si). The corresponding magnetic moments went up from 1.5 and 1.8 to 2.2μ_B. Note that magnetic moments of Mn and other Fe atoms surrounding the defects practically did not change. Hence, the rearrangement of the magnetic states of two Fe atoms, perturbed by the introduction of diamagnetic Si was most likely the reason for the synergetic effect resulting in the strong binding of Mn–Si-dumbbell complex.

Among the configurations listed in Table 1, there is also one in which the synergetic interaction of the FeCr dumbbell and the 1st nn Mn–Si pair resulted in the reduction of the total binding energy. That is the case, when Mn is placed in the compression site next to Cr atom in the dumbbell position. We assign this effect to the antiferromagnetic Cr–Mn repulsion, which is similar to the well known Cr–Cr repulsion in Fe, attributed to the magnetic frustration [25].

The above discussed examples suggest that the interaction of a self-interstitial with the Mn–Si pair is foremost determined by the magnetic contribution rather than strain relaxation. To validate this hypothesis we reveal the effect of cell shape/volume relaxation on the distribution of electronic charge density and magnetic moments in the case of an isolated Mn, Mn–Mn and Mn–Si pairs, and 1st nn Mn–Si pair interacting with the FeFe dumbbell (see Fig. 3a). We took the relaxed (at constant volume) configurations and relaunched a set of calculations optimizing volume and shape of the cell shape but varying the initial magnetic moment on Mn atom(s) from −5 to +5μ_B with an increment of 1μ_B. The reference value of the total energy of the crystal containing a ⟨1 1 0⟩ FeFe dumbbell was also computed to calculate the resulting interaction energy. For the studied configurations, the cell shape/volume relaxation has only a virtual effect on the magnetic moment of Mn and surrounding Fe atoms. The strongest deviation of less than 0.03μ_B was observed for the 1st nn Mn–Si pair. The values of E_I(FeMn–Si) and E_I(FeFe–Mn–Si) shifted down by 0.01 and 0.02 eV, respectively, which is a negligible value. This additional calculations prove adequateness of the constant volume/shape relaxation conditions for the selected problem and confirm the robustness of the results given in Table 1.

4. Conclusions

To summarize, we have studied the interaction of point defects in BCC Fe with Mn–Si and Mn–Si–Cr solute clusters using the spin polarized DFT calculations. The goal of the study was to reveal solute–solute cross-pair interaction and possible synergetic effects in the interaction of solute–defect–solute complexes. Based on the obtained results we draw the following conclusions:

(i) Among the studied solutes only Mn and Si form a weakly stable cross pair in the 1st nn position. This pair exhibits attractive interaction with a vacancy, FeFe and different mixed ⟨1 1 0⟩ dumbbells.

(ii) Several configurations involving Mn, Si and self-interstitial atoms have been relaxed optimizing volume/cell shape. The re-assessed interaction energies and distribution of magnetic moments near the defected zone revealed negligible deviations, proving appropriateness of the constant volume calculations.

(iii) The interaction energy for a self-interaction with the Mn–Si pair varies from ∼0.1–0.8 eV and strongly depends on the local solute arrangement. The strongest binding was observed between an FeFe dumbbell and the 1st Mn–Si pair, which amounted to 0.78 eV. An FeCr dumbbell also exhibits significant binding energy to the Mn–Si pair, which is 0.4 eV. These results suggest that the activation energy for long-range FeFe dumbbell migration in bcc Fe containing Mn and Si, taken as a sum of the migration energy (0.34 eV [15]) and the binding energy, exceeds 1 eV. In the case of the FeCr dumbbell (known to be thermally stable defect), its activation energy for the long-range migration increases up to 0.63 eV (taking 0.23 eV as the migration energy for the FeCr dumbbell [26]).

(iv) The added binding energy due to the insertion of Si next to the FeMn dumbbell is 0.2 eV. Based on the analysis of the charge density maps and local magnetic moments, the origin

of the strong Mn–Si-self interstitial interaction is attributed to the compensation of the magnetic moments of Fe atoms surrounding the dumbbell, occurring due to the perturbation caused by the insertion of diamagnetic Si in ferromagnetic Fe matrix.

(v) The interaction of the Mn–Si pair with a vacancy is less strong than with a self-interstitial atom. The strongest trapping configuration results in the binding energy of 0.34 eV raising the long-range vacancy migration barrier up to 1 eV. This suggests that the trapping of self-interstitials and vacancies at Mn–Si pairs is approximately of the same strength. However, the binding of vacancies to interstitial carbon atoms is even stronger [27].

Following the above conclusions, we would like to put forward that the synergetic interaction of Mn–Si with point defects (not involving Cr), might be responsible for the nucleation of radiation-induced solute-rich complexes associated with growing clusters of point defects. Identification of the role of interstitial carbon and other solutes such as e.g. Ni and P is however needed to complete a complex picture on the elementary interaction of point defects with solutes in Fe-based ferritic steels.

Acknowledgements

This work, supported by the European Commission under the Contract of Association between EURATOM/SCK-CEN, was carried out within the framework of the European Fusion Development Agreement. We are grateful to the ICT Department of Ghent University for partial support of this work. Part of calculations has been performed at HPC Julich within the 'SORT' Project. The research was partly supported by the FWO grant.

References

[1] R.L. Klueh, A.T. Nelson, J. Nucl. Mater. 371 (2007) 37–52.
[2] L. Malerba, G. Bonny, D. Terentyev, E.E. Zhurkin, M. Hou, K. Vörtler, K. Nordlund, J. Nucl. Mater. 442 (2013) 486–498.
[3] L. Malerba, M.C. Marinica, N. Anento, C. Björkas, H. Nguyen, C. Domain, F. Djurabekova, P. Olsson, K. Nordlund, A. Serra, D. Terentyev, F. Willaime, C.S. Becquart, J. Nucl. Mater. 406 (2010) 19–38.
[4] V. Kuksenko, C. Pareige, P. Pareige, J. Nucl. Mater. 432 (2013) 160–165.
[5] V. Kuksenko, C. Pareige, C. Genevois, F. Cuvilly, M. Roussel, P. Pareige, J. Nucl. Mater. 415 (2011) 61–66.
[6] V. Kuksenko, C. Pareige, P. Pareige, J. Nucl. Mater. 425 (2012) 125–129.
[7] V.T. Witusiewicz, F. Sommer, E.J. Mittemeijer, J. Phase Equilib. Diffus. 25 (2004) 346–354.
[8] Z. Jiao, G.S. Was, Acta Mater. 59 (2011) 4467–4481.
[9] T. Klaver, P. Olsson, M. Finnis, Phys. Rev. B 76 (2007) 214110.
[10] P. Olsson, T.P.C. Klaver, C. Domain, Phys. Rev. B 81 (2010) 054102.
[11] E. Vincent, C.S. Becquart, C. Domain, Nucl. Instrum. Methods Phys. Res., Sect. B 228 (2005) 137–141.
[12] E. Vincent, C. Becquart, C. Domain, J. Nucl. Mater. 359 (2006) 227–237.
[13] O.I. Gorbatov, P.A. Korzhavyi, A.V. Ruban, B. Johansson, Y.N. Gornostyrev, J. Nucl. Mater. 419 (2011) 248–255.
[14] A. Bakaev, D. Terentyev, G. Bonny, T.P.C. Klaver, P. Olsson, D. Van Neck, J. Nucl. Mater. 444 (2014) 237–246.
[15] C.-C. Fu, F. Willaime, P. Ordejón, Phys. Rev. Lett. 92 (2004) 175503.
[16] E. Vincent, C. Becquart, C. Domain, J. Nucl. Mater. 351 (2006) 88–99.
[17] C. Domain, C. Becquart, Phys. Rev. B 65 (2002).
[18] G. Kresse, J. Hafner, Phys. Rev. B 47 (1993) 558–561.
[19] G. Kresse, J. Furthmuller, Phys. Rev. B 54 (1996) 11169–11186.
[20] P.E. Blochl, Phys. Rev. B 50 (1994) 17953–17979.
[21] G. Kresse, D. Joubert, Phys. Rev. B 59 (1999) 1758–1775.
[22] J.P. Perdew, J.A. Chevary, S.H. Vosko, K.A. Jackson, M.R. Pederson, D.J. Singh, C. Fiolhais, Phys. Rev. B 46 (1992) 6671–6687.
[23] S.H. Vosko, L. Wilk, M. Nusair, Can. J. Phys. 58 (1980) 1200–1211.
[24] P. Olsson, C. Domain, J. Wallenius, Phys. Rev. B 75 (2007) 014110.
[25] T. Klaver, R. Drautz, M. Finnis, Phys. Rev. B 75 (2006) 094435.
[26] P. Olsson, J. Nucl. Mater. 386–388 (2009) 86–89.
[27] C. Domain, C. Becquart, J. Foct, Phys. Rev. B 69 (2004) 144112.